RESEARCH ARTICLES

J. Frantti,* Y. Fujioka, C. Rouleau, A. Puretzky 2100583

Simulation of the Impact of Point Defects and Edge Dislocations on X-Ray Diffraction in Hexagonal (Ni, Co)$_{1+2x}$Ti$_{1-x}$O$_3$ Thin Films

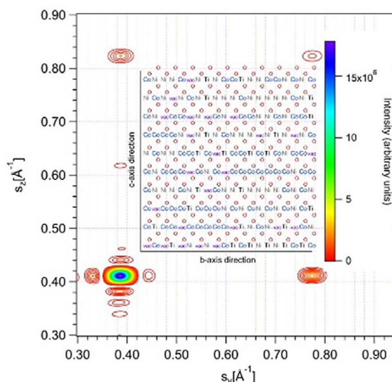

X-ray scattering intensities from clusters with defects are simulated in a desktop computer and compared with experimental data. No profile fitting is applied: the i ntensity is directly computed with minimal approximations. The approach allows to compute scattering intensities from clusters with specified atomic scale structure, size, and shape and can be used for modeling data collected on laboratory X-ray diffractometers.

UNCORRECTED PROOF

physica status solidi b
www.pss-b.com

Simulation of the Impact of Point Defects and Edge Dislocations on X-Ray Diffraction in Hexagonal $(Ni,Co)_{1+2x}Ti_{1-x}O_3$ Thin Films

Johannes Frantti, Yukari Fujioka, Christopher Rouleau, and Alexander Puretzky*

A computer code for simulating high-resolution X-ray diffraction (XRD) data from disordered crystals with arbitrary spatial composition and local lattice parameters is developed. Simulated patterns are compared with the experimental data collected on a single phase, highly crystalline $(Ni_{0.42}Co_{0.58})_{2.22}Ti_{0.39}O_3$ solid-solution thin film exhibiting a large number of subsidiary minima. As a case study, the edge dislocations in hexagonal $(Ni,Co)_3O_3$ thin films with Burgers vector parallel and perpendicular to the *a*-axis and *c*-axis, respectively, are modeled. No peak profiles are assumed and thus issues related to profile fitting are avoided. Both macroscopic features, such as film thickness and atomic scale structure, such as dislocations, are simultaneously modeled. Simulations are run on a desktop machine. Commonly applied database-based phase identification routines can result in wrong phase identification, unless intensities are properly modeled. Modeling tools of diffractometer manufacturers are compared with the present approach. An example of how simulated reciprocal lattice patterns can be used to choose relevant measurement geometries in defected thin films is given.

1. Introduction

Understanding and controlling crystal defects are essential in material engineering, the classical example being semiconductor devices created by a spatially well-controlled point defect distribution.[1] 2D defects include domain wall and grain boundaries. Polarization reversal in ferroelectric materials is essentially dictated by domain walls, whose dynamics can be highly complex.[2] The meaning of domains and domain boundaries for the polarization reversal in ferroelectrics is as crucial as the role of dislocations for the plasticity of metals.[3]

Edge dislocations are classified as line defects which are frequently formed in strained thin films. In case the lattice mismatch exceeds the critical value, edge dislocations are formed. After exceeding the critical thickness, the lattice parameters relax to their natural values. A spatially extended displacement field accompanies dislocation, which in diffraction measurements is often seen as an asymmetric line shape. Determination of the strain and dislocation density are key parameters in semiconductor devices based on the epitaxial thin films.

Crystal defects have a decisive role for the properties of thin films, yet their nondestructive structural characterization is challenging as the volume is characteristically small and the films are grown on a substrate. X-ray diffraction (XRD) is the prevailing route for nondestructively characterizing crystals and their defects.[4–7] XRD analysis relies on results extracted from bulk samples, single crystals, and powders. XRD data collected on thin-film samples possessing several layers are commonly considered to be consisting of noninteracting layers, the result being a sum of the patterns from each layer (or phase). To estimate the phase fractions, standard profile functions (e.g., Lorentz, Pearson or pseudo-Voigt) are commonly applied to model reflection intensities. The approach suits for the polycrystalline materials lacking features resulting from long-range order (e.g., subsidiary peaks in thin films) but is an overly coarse approach for highly ordered nanoscale structures. For instance, while asymmetric line shapes can routinely be fit by the standard line profiles, it is often hard to ascertain the origin of the asymmetry.

In this article, another approach is taken to model defected films. The films, with spatially varying composition and structure, are taken as a single scattering unit. As the dimensions are small, between 10 and 100 nm, the scattered X-ray intensity profile is to an excellent accuracy determined by the sample, and no preassumed profile function is applied. We first simulate diffraction patterns from the homogeneous $(Ni_{0.42}Co_{0.58})_{2.22}Ti_{0.39}O_3$ film possessing atomic-scale disorder and second from hexagonal $(Ni,Co)_3O_3$ thin films under compressive biaxial strain and edge dislocations. The situation contrasts to the case where no stress relaxation by dislocation has taken place. Thus, the simulations suit for cases where the standard measurements in which *d*-spacing for a chosen reflection *hkl* measured from a polycrystalline film is plotted as a function of tilt angle ψ (d_{hkl} vs $\sin^2\psi$ plot) are not applicable. Finally, a discussion of the commonly available modeling tools available from

J. Frantti, Y. Fujioka
Finnish Research and Engineering
Jaalaranta, Helsinki 00180, Finland
E-mail: Johannes.frantti@fre.fi

C. Rouleau, A. Puretzky
Center for Nanophase Materials Sciences
Oak Ridge National Laboratory
Oak Ridge, TN 37831, USA

The ORCID identification number(s) for the author(s) of this article can be found under https://doi.org/10.1002/pssb.202100583.

DOI: 10.1002/pssb.202100583

UNCORRECTED PROOF

© 2022 Wiley-VCH GmbH

commercial diffractometer manufacturers is given, with the intent to relate the present approach with these modeling tools.

2. Template Structures

The hexagonal structure was used as a template to simulate diffraction from $(Ni_{0.42}Co_{0.58})_{2.22}Ti_{0.39}O_3$ clusters (discussed in Section 3.1) and from $(Ni,Co)_3O_3$ clusters (discussed in Section 3.2) with an edge dislocation. The initial simulation cluster is given in terms of the number of cell (defined below) replicas in each orthogonal direction, after which the cluster is modified as desired (e.g., by mixing cations, introducing vacancies, strained layers and dislocations, and thus making the cells unequal). Finally, the scattering intensity is computed for a given direction or plane so that the simulations can be compared with experiments.

2.1. Hexagonal $(Ni,Co)_3O_3$

$(Ni,Co)_3O_3$ crystallizes in the space group symmetry no. 194. Nickel and cobalt cations are at $2a$ sites and oxygen at $2c$ sites. Oxygen is arranged in the hexagonal close-packed structure, and nickel and cobalt occupy the octahedral interstices. Details are given in other studies.[8,9] In simulations, orthohexagonal-centered cell C_1, defined in the study by Arnold et al.,[10] was applied and is termed as "cell." For the ease of comparison, reflections are expressed in terms of the hexagonal axes. We note that a and c axes of the C_1 and triple-hexagonal cell are the same. Experimentally, the hexagonal structure exhibits only $003l$, l even reflections. The cell contains four octahedrally coordinated cation sites and four oxygen. The cation sites can all be occupied, as in the case of $(Ni,Co)_3O_3$, or some can be vacant, as in the case of the $(Ni_{0.42}Co_{0.58})_{2.22}Ti_{0.39}O_3$.

2.2. Titanium-Alloyed Sample

The crystal structure of $(Ni_{0.42}Co_{0.58})_{2.22}Ti_{0.39}O_3$ is obtained from the $(Ni,Co)_3O_3$ structure by replacing two 2+ cations by one Ti^{4+} and one cation vacancy. If all four species, Ni^{2+}, Co^{2+}, Ti^{4+}, and vacancies, were randomly and homogeneously distributed over the octahedral sites, the average would be the hexagonal structure. Experiments show that Ti^{4+} alloying results in the appearance of $003l$, l odd reflections. This is consistent with the notion that the octahedra layers alternating along the c-axis direction are not equivalent.

3. X-ray Scattering Simulations

XRD patterns collected on oriented films frequently possess only few reflections. Films with good crystallinity exhibit a large number of well-resolved subsidiary minima. When the average composition is known, rather, detailed models can be justified by XRD patterns. The intensities and positions of the subsidiary minima contain information on film thickness and cation and vacancy distribution, complementing the information extracted from the primary peaks.

3.1. Simulation of the Intensity Scattered from $(Ni_{0.42}Co_{0.58})_{2.22}Ti_{0.39}O_3$ Film

One of the samples reported in the study by Fujioka et al.,[9] labeled as sample H, was selected to compare the experimental and simulated data. 74% of the octahedra interstices were occupied by Ni^{2+} and Co^{2+} (Ni/Co ratio 42/58), 13% by Ti^{4+}, and 13% of the octahedra interstices were vacant. Estimates are based on the composition analysis reported in the study by Fujioka et al.[9] Due to the different cation charges and sizes, the composition is expected to vary in atomic scale. To account for this in the simulation, two compositionally slightly different layers alternate along the c-axis direction. In each layer, Ti^{4+} and vacancy fraction were constrained to be equal, and the Ni/Co ratio was 42/58. Within each layer, the distributions of the cations and vacancies were randomized. The overall composition was constrained to the experimentally determined value. While the model is simple, it is able to grasp the essential features. The octahedra filling factor and cation distribution can also be altered in the bulk $(Ni_{1-x}Co_x)TiO_3$ materials, though to a lesser extent than in thin films.[11] Cation distribution severely affects the physical properties, such as magnetization.[12]

Figure 1 shows the XRD pattern measured from the $(Ni_{0.42}Co_{0.58})_{2.22}Ti_{0.39}O_3$ (sample H in other studies[8,9]) film together with the simulated pattern. The diffracting beam was dominantly $K\alpha_1$ radiation, with a minor contribution from $K\alpha_2$ radiation. Indexing refers to hexagonal axes, in which the indices corresponding to the ilmenite structure are given. Both simulations and experiments reveal strong 006 and 0012 reflections and significantly weaker 003 and 009 reflections. The 003 and 009 reflections are absent in $(Ni,Co)_3O_3$ samples in which all octahedra are randomly occupied by Ni and Co (sample E in other studies[8,9]). This was confirmed by simulations (not shown). The intensities, however, show that the cation distribution in sample H significantly deviates from the ilmenite structure. By redistributing the cations, the odd reflections can be tuned off or adjusted to finite values.

Simulations indicate that subsidiary minima are a sensitive function of cation distribution and the cluster size, as seen from the fluctuation in subsidiary minima intensities between simulations based on different cluster sizes. This is characteristic to the case where the long-range order is not rigorously obeyed in the film plane and is a feature clearly seen when small cluster sizes are applied in the simulation. To put the simulation consistent with the experimental observation, 12 clusters, each of size $12 \times 1 \times 118$ with 11 328 atoms (counting vacancies as atoms), were constructed. Correspondingly, the thickness was $118 \times 4.858432\,\text{Å} \approx 57.3\,\text{nm}$. Previously, a nonconstrained Gaussian fit to subsidiary minima and a subsequent fit of the minima positions yielded an estimate of 53.7 nm.[9] The experimentally observed quality of the subsidiary minima indicated that also the in-plane coherence length is good: the larger the cluster projection on the substrate plane, the better the subsidiary minima are revealed. As the cations and vacant octahedra were not ordered, the subsidiary minima intensities between different clusters vary, as is most clearly seen in the small 2θ range, as shown in Figure 1. Experimentally recorded 003 reflection did not reveal clear subsidiary minima, consistently with

UNCORRECTED PROOF

© 2022 Wiley-VCH GmbH

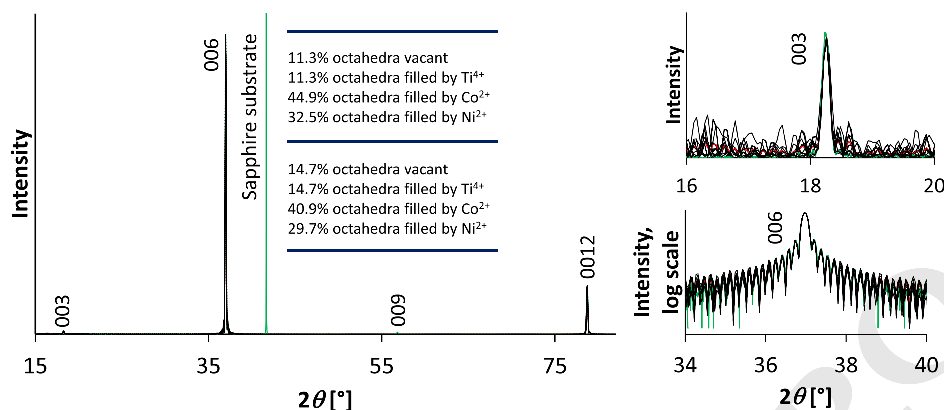

Figure 1. Simulations and experimental XRD intensities measured from sample H. Green line shows the experimental data. Dotted lines give the contributions from 12 individual clusters, and red line is their average.

simulations. Simulations show that the intensity from individual clusters at the small 2θ range are scattered around the average value.

The 006 and 0012 reflections, including subsidiary minima, are in agreement with the experimentally determined profiles. The experimentally observed 003 and 009 reflections are two orders of magnitude weaker and the simulated and experimental intensities of the 009 reflection (possessing <0.7% of the intensity of the 006 reflection) were underestimated. The model was kept simple by aiming at the minimal number of structural parameters. The main features, however, agree with experiments.

3.2. Edge Dislocation Displacements in $(Ni_{0.50}Co_{0.50})_3O_3$ Film

The displacement field outside the dislocation line resulting in edge dislocation is summarized in Supporting Information. The scattering cluster is considered to consist of slices schematically shown in Figure S1, Supporting Information. To estimate the effect of the displacement fields on the diffraction patterns, displacements given by Equation (21) and (22), Supporting Information were introduced to the atomic positions of the initially created cluster. It is worth mentioning that it is the long-range displacement field, triggered by the excess atomic plane in Figure S1, Supporting Information, which modifies the X-ray scattering intensities. The direct contribution of the excess atomic plane itself is rather small.

We consider cases in which the edge dislocation lines are parallel either to the *a*-axis or the *c*-axis. The dislocation line positions and directions are given in terms of the lattice vectors and were assumed to be statistically distributed along the slip plane. Scattering intensity was computed for each dislocation line position. In both cases, the starting point was a cluster generated from the $(Ni_{0.50}Co_{0.50})_3O_3$ structure, given in Section 2, in which Ni^{2+} and Co^{2+} cations were ordered over the octahedra interstices. The cluster contained a 7.82 nm-thick layer, in which the *c*-axis length was 4.8900 Å. The layer presents a compressively strained layer. The relaxed *c*-axis length value was 4.8703 Å. Prior to the introduction of the dislocation-generated displacement field, the *a*- and *b*-axis lengths were 2.980300 Å and 5.162231 Å, respectively. The cluster size in both cases was $1 \times 23 \times 45$, corresponding to the cluster size 0.3 nm × 11.9 nm × 22.0 nm and 8280 atoms. In all simulations, Poisson ratio was fixed to 0.30.

Figure 2 shows the simulated pattern corresponding to the case in which the dislocation line is parallel to the *x*-axis, *xy*-plane is the slip plane, and the excess atom plane is *xz*-plane. The dislocation is termed *x*-dislocation and corresponds to a common stress relieve model in which in-plane stress is relaxed by edge dislocations. The Burgers vector length was equal to the hexagonal *a*-axis length. Both 00*l* and 0*k*0 reflections, shown in Figure 2a, are asymmetric.

The impact of the second dislocation type, termed *z*-dislocation, is shown in **Figure 3**. In this case, the excess atom plane generating the displacement field is parallel to the film surface. As in the *x*-dislocation case, 00*l*-reflections are asymmetric, whereas the 0*k*0-reflections remain fairly symmetric, as shown in Figure 3b. The Burgers vector was set to $c/4$. We speculate that such a situation could be formed during film growth as the material is consists of oxygen octahedra blocks possessing Ni or Co. Also, each oxygen is coordinated by six metal cations. Even though the geometrical shapes of the cation and oxygen octahedra are different, it is worth to note that by swapping cations and anions, the *z*-coordinates are changed by one-quarter of the *c*-axis length. An interesting consequence is that the *z*-dislocation generates atomic-scale terraces and thus would accelerate thin-film growth speed. To our experience, films grow on $LiNbO_3$ (tensile in-plane strain) and GaN (compressive in-plane strain) significantly faster than films on Al_2O_3. The role of dislocation is to be clarified.

The two dislocation types can be distinguished by measuring both 0*k*0 and 00 *l* reflections. In the case of *z*-dislocations, the 0*k*0 reflections remain symmetric, while they are asymmetric in *x*-dislocation case.

3.3. Note on Displacement and Cation Arrangement Disorder

Figure 2c and 3c show 00 *l*, *l* odd, reflections. The prime cause of the reflections is the ordered way the Ni and Co cations were distributed, as illustrated in Figure 2d and 3d. Intensities were

UNCORRECTED PROOF

© 2022 Wiley-VCH GmbH

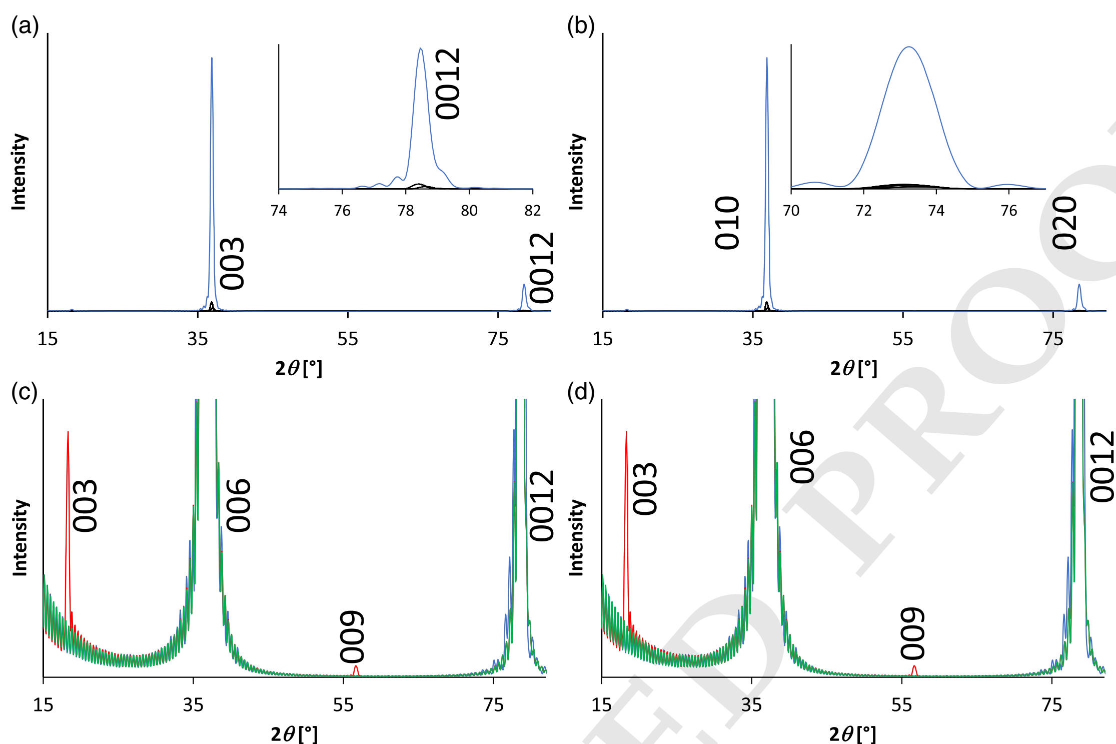

Figure 2. Simulated scattering intensities for *c*-axis-oriented film possessing *x*-dislocations. Panels (a) and (b) show 00*l*- and 0*k*0-type reflections, respectively. Panel (c) reveals weak 003 and 009 reflections. The reflections disappear when Ni and Co are randomly distributed, see blue (*x*-dislocation line at positions $y = 3b$ and $z = 15c$) and green lines (dislocation-free cluster) in panel (d). Pattern from a dislocation-free cluster with ordered distribution of Ni and Co is shown by a red line.

also affected by the position of the dislocation line, due to the dislocation-generated displacements. Reflections are roughly two orders of magnitude weaker than 00*l* reflections with even *l* and disappear when cobalt and nickel are randomly distributed. Merely counting the reflections and their positions present in the pattern can result in a wrong structural model. For instance, in the present case, the positions (but not the intensities) match with the ideal ilmenite structure and care must be exercised when database-based phase identification is applied.

The present simulations assumed a rather high dislocation density, which can occur during film growth. Small dislocation densities require large simulations cells.

4. Notes on the Modeling Tools Available in Commercial Diffractometers

Commercial diffractometers can typically be configured for XRD, high-resolution X-ray diffraction (HRXRD), and X-ray reflectometry (XRR) measurements. While XRD and HRXRD suit crystal structure, strain, strain gradient, and even crystallite dimension along the perpendicular (thickness) and parallel (in-plane) directions in the case of thin, well-oriented and highly crystalline films, XRR is the standard tool for estimating the film thickness, film density along the thickness direction, and surface (interface) roughness. XRR is a scattering, in contrast to diffraction, technique essentially dictated by macroscopic-scale densities and interfacial roughness, and the models are different from the models applied in XRD data analysis. XRR modeling is not based on the atomic-scale structure and suits also for characterizing amorphous films. For a summary of XRR modeling, see, for example, other studies.[5,13]

4.1. XRD Data Modeling Tools

Diffractometer manufacturers provide a rich set of data manipulation and modeling tools, based either on the standard X-ray diffraction intensity theory or on the macroscale models not directly considering the atomic-scale structure.

The first mentioned usually starts with a cell generation tool in which the initial parameters are given by specifying the asymmetric unit and space group. Information about defects is then obtained by adjusting profile function parameters to match the experimental data. The profile function parameters contain the information about crystal defects, the peak positions, and areas being dictated by the crystal structure. For example, solid solution is modeled by a cell with pseudoatoms formed from composition weighed averages of the constitute atoms sharing the same crystallographic site.

Examples of the macroscale models are tools dedicated for the analysis of film thickness, surface roughness, and strain state in polycrystalline films. A standard method for analyzing the strain state of polycrystalline films is based on the measurement of differently oriented *hkl* planes by forming the d_{hkl} versus

UNCORRECTED PROOF

© 2022 Wiley-VCH GmbH

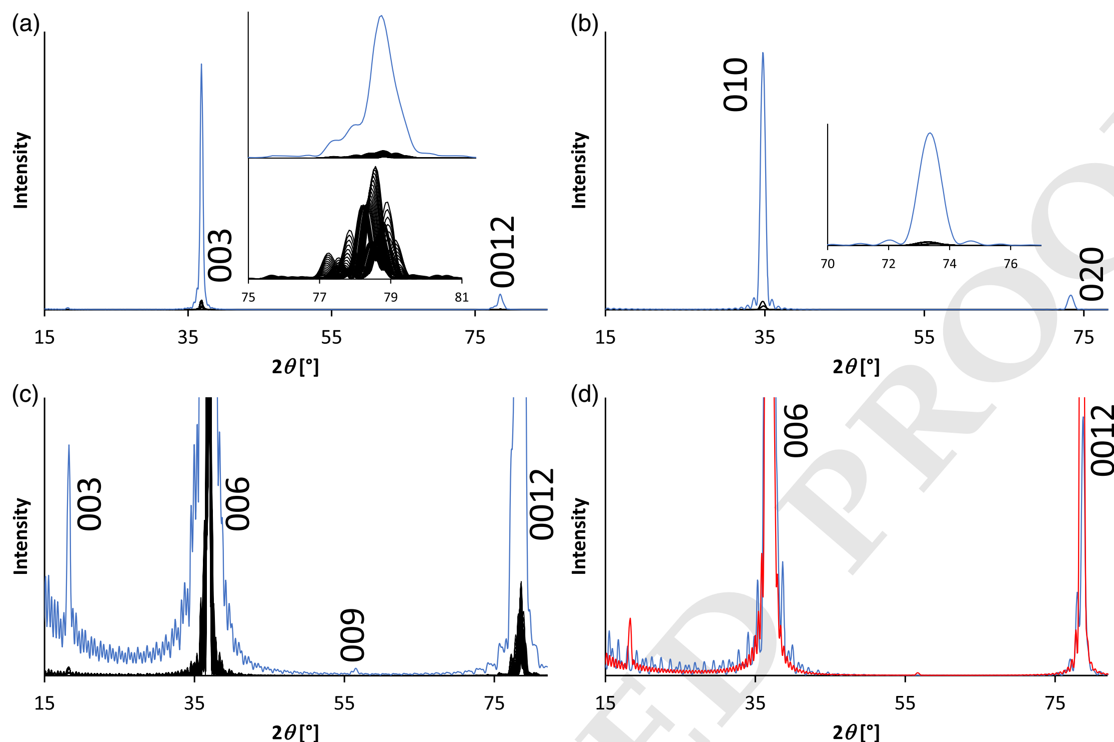

Figure 3. Simulated scattering intensities for c-axis-oriented film possessing z-dislocations. Panels (a) and (b) show $00l$ and $0k0$ reflections, respectively. Scattering contribution from the individual clusters is shown in the insets for 0012 reflection. Panel (c) reveals weak 003 and 009 reflections. The reflections disappear when Ni and Co are randomly distributed, see blue line (z-dislocation line at $y = 3b$ and $z = 15c$) in panel (d). Pattern from a dislocation-free cluster with ordered distribution of Ni and Co is shown by a red line.

$\sin^2\psi$ plot. Most diffractometer manufacturers provide strain analysis tools, though the method does not suit for highly oriented or epitaxial films.

When data modeling tools are aimed for fast, even in situ analysis of the data, tools need to be simple. Correspondingly, prevailing methods are based on the determination of the center position and width of the chosen reflection(s). These parameters are commonly determined by fast and straightforward techniques, including the determination of the center of gravity, centered center of gravity, parabola fit, and the profile fit to experimental data.

However, the profile can be and in practice always is a result of different contributions, which are not necessarily adequately modeled by the simple center position estimation techniques. This is a critical stage as whatever is being measured, let it be peak shifts, is generally a function of different factors such as strain, composition gradients, and complex atomic displacements following edge dislocations. While being convenient, the software which takes care of the various data processing stages may in practice be a blackbox modeling, with a risk that the tools are applied to unjustified cases.

4.2. Applications of the Present Approach

We simulated the relatively straightforward, symmetric θ–2θ measurement case. This is to be compared with the grazing-incidence XRD (GIXRD) measurements where the instrumental corrections required to be properly taken into account are more involved. However, when the intensities are computed within the kinematic theory, the computation of diffraction intensities follows the same lines as in the present work. The benefit of GIXRD is its ability to give thickness-dependent information and thus allow a closer relation between simulation and experiments. The highest-quality, homogeneous thin films may require the modeling through the dynamic theory. Even these cases rarely entirely correspond to the predictions of the dynamic theory and data have to be modeled in a case-by-case manner.

What we suggest is to test the validity of the model prior to applying the aforementioned tools. The purpose of the present work is to show that any atomic-scale structure (including structures possessing no translational symmetry) with arbitrary shape and size within the limits of typical thin-film thicknesses (say, up to few hundred nm) can easily and accurately be simulated to match with the high-resolution X-ray scattering data. This is essentially due to the significantly improved computational power. Perhaps the greatest appealing feature of the present approach is the direct link between the scattering cluster and scattering intensity. An example of a case where straightforward modeling may give a misleading result is the thickness estimation. As the crystallite dimension along the perpendicular direction is equal to the thickness only in the thinnest and highest quality epitaxial films, the estimate by the well-known Scherrer equation should be adopted with caution, particularly if the sample contains defects. Another example where

UNCORRECTED PROOF

© 2022 Wiley-VCH GmbH

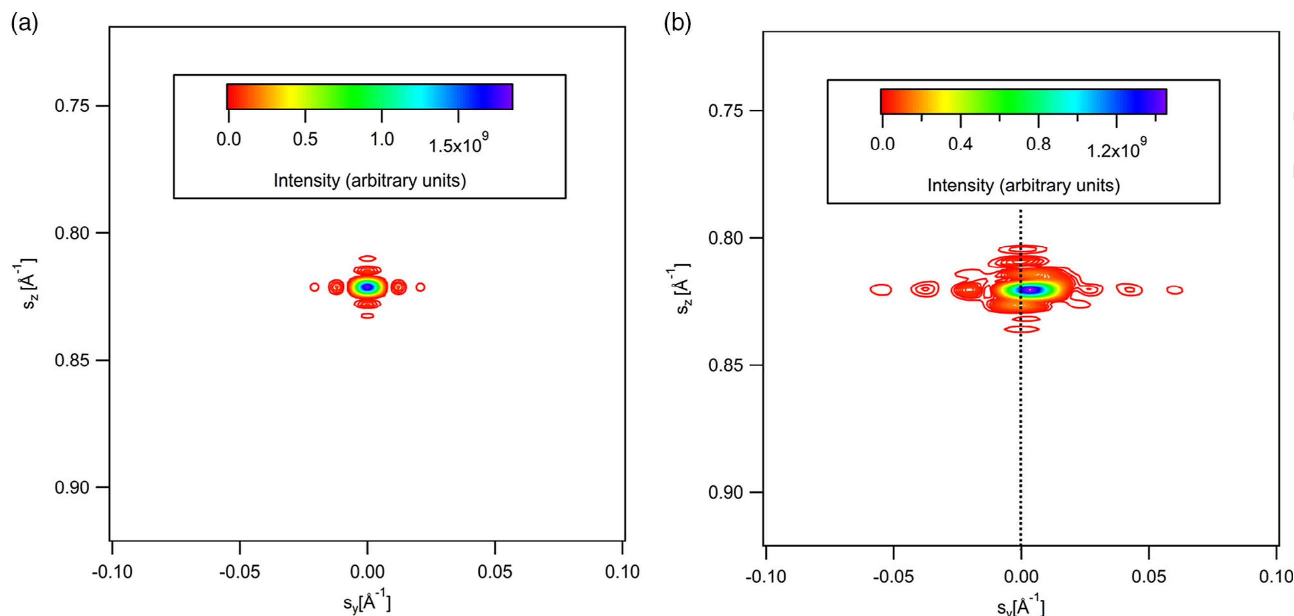

Figure 4. Simulated scattering intensities from the $s_x = 0$ plane of a $1 \times 23 \times 45$ cluster in a) defect-free cluster and b) from a cluster with a strained layer and *x*-dislocation line. Dotted vertical line corresponds to the abscissa in Figure 2c.

traditional modeling tools may not be adequate are data collected on devices fabricated on a wafer. The collection of devices forms a 3D structure possessing no long-range order. As the location and structure of the devices are fairly accurately known, XRD techniques are applicable.

As a final example, we illustrate how plotting intensities in reciprocal planes provides a practical route to see peak width distribution and thus helps design appropriate experiments. Reciprocal mapping is routinely available in HRXRD diffractometers. **Figure 4** compares XRD intensities from a defect-free $1 \times 23 \times 45$ $(Ni,Co)_3O_3$ cluster with the same size cluster possessing an *x*-dislocation line at position $y = 3b$, $z = 15c$ and a strained layer. The cluster is the same as was used in the simulation shown in Figure 2c. In defect-free cluster, the 0012 reflection along the s_y-direction is clearly broader than along the s_z-direction. The intensity distribution is spread and asymmetrically distributed due to the strained layer and a dislocation. Many contemporary X-ray diffractometers can be configured for both in-plane and out-of-plane diffraction measurements, so that a comparison between the simulation and experiments can be conducted.

In the case of complex structures, the challenge is to find good initial values to be refined with reasonable computational effort. While XRD measurements do provide ample amount of information, they may not always be sufficient for a correct structure determination. Thus, the present approach is practical when one has decent a priori model of the sample, and the goal is to test or validate the model. In this case also structural refinement is feasible. This covers rather broad range of technically important properties, such as composition distribution, different dislocations, surface roughness, mosaicity and the estimates of crystal plate size and thickness in single and multilayer structures. Obviously, the increase of computational power allows to expand direct computation approach to more complex systems. If instrumental line broadening is significant, a fundamental parameter approach can be applied to differentiate the instrumental and sample broadening.[14]

A further advantage is the possibility to use the same scattering cluster for neutron scattering studies, especially for studying magnetic scattering.

5. Conclusion

Both detailed macroscopic and atomic-scale information can be extracted from a high-resolution X-ray diffraction data collected on weakly disordered, oriented thin films through a single simulation. Desktop computers possess sufficient amount of capacity to simulate high-resolution intensity collected on standard, commercially available X-ray diffractometers. No line shape function was assumed, in contrast to profile-fitting approaches. Case studies included weakly disordered thin films with randomly distributed spatial point defects and edge dislocations combined with a strained layer. Simulation is a practical tool for distinguishing the effect of different disorder types to X-ray diffraction patterns and can be used both for experiment planning and experimental data modeling. Computational capacity has increased so that detailed simulations of the planar devices integrated on semiconductor chips can also be modeled.

6. Experimental Section

A C++ computer code utilizing OpenMP directives was written to generate a scattering cluster and compute X-ray scattering intensity. Initially, the cluster can and was typically constructed from identical cells by piling them in three spatial directions, and the composition and cell size were subsequently altered. In the case of weak disorder, we still use terms

UNCORRECTED

© 2022 Wiley-VCH GmbH

lattice vector, etc., even though the translational symmetry was not strictly obeyed. For the alteration, a set of manipulations tools, for instance, allowing to displace atoms as desired, mix them (e.g., to form a solid solution including vacancies or to place solute atoms to a dislocation line), and to create dislocations and tilted volumes within the cluster was implemented. Vacancies allowed to introduce an atomic-scale surface roughness. Atomic positions were generated that also magnetic scattering from arbitrary spin configuration could straightforwardly be implemented. Coefficients for analytical approximation to the X-ray scattering factors f were adapted from the study by Brown et al.[15] Once the atomic positions were specified, the intensities were computed as described in other studies.[16,17] To compare simulations with the experimental data, appropriate polarization and Lorentz factors were applied.[7] Standard θ–2θ measurement geometry was assumed. To allow a comparison with experimental data, scattering intensity was presented as a function of 2θ, assuming $K\alpha_1$ radiation. $K\alpha_2$-contribution was included, though its contribution was not significant. Intensity in the reciprocal lattice points was given in terms of vector components of $\mathbf{s} = (\mathbf{S} - \mathbf{S}_0)/\lambda$, where $\mathbf{S}$ and $\mathbf{S}_0$ are the unit vectors indicating the directions of the scattered and incident X-rays, respectively, and λ was the wavelength of the X-rays.

Supporting Information

Supporting Information is available from the Wiley Online Library or from the author.

Acknowledgements

All experimental work was conducted at the Center for Nanophase Materials Sciences (CNMS), which is a DOE Office of Science User Facility. The authors thank Dr. Jong Keum (Oak Ridge National Laboratory) for his help with X-ray diffraction measurements conducted at CNMS. The project was financed by Reciprocal Engineering—RE Ltd. RE is a Helsinki, Finland-based company, which develops new magnetic thin-film materials functional at and above room temperature for semiconductor industry.

Conflict of Interest

The authors declare no conflict of interest.

Data Availability Statement

Data sharing is not applicable to this article as no new data were created or analyzed in this study.

Keywords

defects, diffraction, edge dislocations, hexagonal, scattering, simulation, thin films

Received: November 12, 2021
Revised: January 18, 2022
Published online:

[1] K. F. Brennan. *Introduction to Semiconductor Devices for Computing and Telecommunications Applications*, Cambridge University Press, Cambridge, UK **2010**.
[2] M. E. Lines, A. M. Glass. *Principles and Applications of Ferroelectrics and Related Materials*, Oxford University Press, Oxford, UK **2001**.
[3] *Numerous reports interpret the polarization reversal (and many other types of anomalies in the measurements data) in terms of a straightforward "polarization rotation" without considering the domain wall motion*. This is discussed in J. Frantti, Y. Fujioka, R. M. Nieminen. J. Phys.: Condens. Matter. 2008, 20, 472203; J. Frantti, Y. Fujioka, R. M. Nieminen. J. Phys. Chem. B 2007, 111, 4287.
[4] A. Guinier, *X-ray Diffraction in Crystals, Imperfect Crystals, and Amorphous Bodies*, Dover Publications, Inc., New York **1994**.
[5] M. Birkholz. *Thin Film Analysis by X-Ray Scattering*, Wiley-VCH Verlag GmbH & Co. KGaA, Weinheim **2006**.
[6] L. S. Zevin, G. Kimmel. *Quantitative X-ray Diffractometry*, Springer-Verlag, New York **1995**.
[7] W. Massa. *Crystal Structure Determination*, Springer-Verlag, Berlin Heidelberg **2000**.
[8] Y. Fujioka, J. Frantti, C. Rouleau, A. Puretzky, Z. Gai, N. Lavrik, A. Herklotz, I. Ivanov, H. Meyer, *Ann. Phys.* **2019**, *531*, 1900299.
[9] Y. Fujioka, J. Frantti, C. Rouleau, A. Puretzky, H. Meyer, *Phys. Status Solidi B* **2017**, *254*, 1600799.
[10] H. Arnold, in *International Tables for Crystallography, Volume A: Space-group symmetry* (Ed.: Th. Hahn), Kluwer Academic Publishers, Dordrecht, The Netherlands **2005**.
[11] Earlier Raman scattering study indicated that $Ni_{1-x}Co_xTiO_3$ ceramics undergo a reversible, high-temperature order-disorder phase transition – a transition between the ilmenite-corundum structures – which necessitates cation diffusion via the vacant octahedra sites. Now, once the sample is cooled, the perfect vacant octahedra order required by the ilmenite structure is not fully reached, which results in lower crystal symmetry seen by Raman scattering (see Y. Fujioka, J. Frantti, A. Puretzky and G. King. Inorganic Chemistry. 2016, 55, 9436) and diffraction studies (Y. Fujioka. J. Frantti, A. Llobet, G. King and S. Ehrlich. Materials Today: Proceedings 2016, 3, 265.). The low-frequency band observed by Raman scattering is consistent with our phonon computations (unpublished).
[12] J. Frantti, Y. Fujioka, C. Rouleau, A. Steffen, A. Puretzky, N. Lavrik, I. N. Ivanov, H. M. Meyer, *J. Phys. Chem. C* **2019**, *123*, 19970.
[13] I. D. Feranchuk, S. I. Feranchuk, L. Komarov, S. Sytova, A. Ulyanenkov. *Phys. Rev. B* **2003**, *67*, 235417.
[14] R. W. Cheary, A. Coelho, *J. Appl. Cryst.* **1992**, *25*, 109.
[15] P. J. Brown, A. G. Fox, E. N. Maslen, M. A. O'Keeffe, B. T. M. Willis, in *International Tables for Crystallography, Volume C: Mathematical, Physical and Chemical Tables* (Ed. E. Prince), Kluwer Academic Publishers, Dordrecht, The Netherlands **2002**.
[16] J. Frantti, Y. Fujioka, *Ann. Phys.* **2015**, *527*, 219.
[17] J. Frantti, Y. Fujioka, EP2464962, **2014**.
[18] E. Kaxiras. *Atomic and Electronic Structure of Solids*, Cambridge University Press, Cambridge **2003**.
[19] S. Timoshenko, J. N. Goodier. *Theory of Elasticity*, McGraw-Hill Book Company, New York **1951**.
[20] R. Phillips. *Crystals, Defects and Microstructures: Modeling Across Scales*, Cambridge University Press, Cambridge **2001**.
[21] A. Kelly, K. M. Knowles, *Crystallography and Crystal Defects*, 2nd ed., Wiley, Malaysia **2012**.

UNCORRECTED PROOF

© 2022 Wiley-VCH GmbH